

## Microstructural and Compositional Characterisation of Electronic Materials

D.V. Sridhara Rao<sup>1,\*</sup>, R. Sankarasubramanian<sup>1</sup>, Deepak Kumar<sup>1</sup>, V. Singh<sup>1</sup>,  
K. Mahadeva Bhat<sup>#</sup>, P. Mishra<sup>#</sup>, S. Vinayak<sup>#</sup>, T. Srinivasan<sup>#</sup>, R. Tyagi<sup>#</sup>,  
K. Muraleedharan<sup>@</sup>, R. Muralidharan<sup>§</sup>, and D. Banerjee<sup>^</sup>

<sup>1</sup>Defence Metallurgical Research Laboratory, Hyderabad - 500 058, India

<sup>#</sup>Solid State Physics Laboratory, Delhi - 110 054, India

<sup>@</sup>Central Glass Ceramic Research Institute, Kolkata 700 032, India

<sup>§</sup>Center for Nanoscience and Engineering, Indian Institute of Science, Bengaluru - 560 012, India

<sup>^</sup>Department of Materials Engineering, Indian Institute of Science, Bengaluru - 560 012, India

\*E-mail: dvsridhararao@gmail.com

### ABSTRACT

Microstructural and compositional characterisation of electronic materials in support of the development of GaAs, GaN and GaSb based multilayer device structures is described. Electron microscopy techniques employing nanometer and sub-nanometer scale imaging capability of structure and chemistry have been widely used to characterise various aspects of electronic and optoelectronic device structures such as InGaAs quantum dots, InGaAs pseudomorphic (pHEMT) and metamorphic (mHEMT) layers and the ohmic metallisation of GaAs and GaN high electron mobility transistors, nichrome thin film resistors, GaN heteroepitaxy on sapphire and silicon substrates, as well as InAs and GaN nanowires. They also established convergent beam electron diffraction techniques for determination of lattice distortions in III-V compound semiconductors, EBSD for crystalline misorientation studies of GaN epilayers and high-angle annular dark field techniques coupled with digital image analysis for the mapping of composition and strain in the nanometric layered structures. Also, *in-situ* SEM experiments were performed on ohmic metallisation of pHEMT device structures. The established electron microscopy expertise for electronic materials with demonstrated examples is presented.

**Keywords:** Electronic materials, semiconductor electronic device, nanowires, infrared device structure

### 1. INTRODUCTION

Electron microscopy is one of the important characterisation tools for structural and compositional characterisation of electronic materials and semiconductor device structures. In several cases, the device structures are in the form of multilayered thin films with heteroepitaxial interfaces. Some examples are: high-electron mobility transistors (HEMTs) and infrared (IR) photodetectors<sup>1,2</sup>. The HEMTs find applications in low-noise amplifiers, SPDT switches, phase shifters and attenuators (working at microwave frequencies) used in phased array radars, wide band communications and ground communications. The photodetectors, based on either InGaAs quantum dots or GaSb/InAs type-II superlattice structures are useful for infrared applications. In many of these devices, the thickness of epilayers is in the micrometer-nanometer scale and the investigation of different microstructural parameters, such as thickness of individual epilayers, microstructural defects (viz., dislocations, stacking faults, etc), lattice strain/coherency across multilayers, polarity, surface modulations and compositional homogeneity are very important. Also, the HEMT device programs involve the development of thin

films structures for ohmic metallisation, resistors, dielectrics etc. For the investigation of these nanoscale issues, electron microscopy techniques are ideally suited.

In this review, authors presented an overview of investigating the microstructural and compositional studies of the semiconductor electronic device structures, primarily by employing electron microscopy (scanning electron microscopy-SEM and transmission electron microscopy-TEM) techniques. The device structures are grown by a wide range of thin film deposition techniques. In this regard, the initial studies on the electron microscopy characterisation of buffer layers (AlGaAs/GaAs superlattices, low-temperature GaAs and InAlAs metamorphic buffers) and InGaAs quantum dots were documented in our earlier published work<sup>3</sup>. In due course of time, the necessary infrastructure and expertise for conducting electron microscopy investigations of electronic materials have been established in the functional areas of:

- plan-view and cross-sectional TEM specimen preparation of semiconductor thin films<sup>4</sup>
- site-specific TEM specimen preparation of electronic devices
- TEM imaging conditions for epitaxial layers of III-Arsenides and III-Nitrides
- convergent beam electron diffraction (CBED) based

- techniques for quantitative lattice distortion studies in III-V thin films & polarity of GaN based films<sup>5,6</sup>
- (e) quantitative strain/compositional studies of epitaxial thin films by the digital analysis of HRTEM images<sup>7</sup>
  - (f) quantitative analysis of heterointerfaces by atomic-column ratio mapping
  - (g) *in-situ* SEM studies, and
  - (h) compositional analysis by EDS and EELS techniques.

An overview of GaAs, GaSb and GaN multilayer semiconductor device structures and the application of advanced electron microscopy techniques to study various issues in these materials development programs are presented.

## 2. GaAs HEMT DEVICE STRUCTURES

HEMT is a field effect transistor in which the channel is a quantum well (QW) realised by embedding a narrow bandgap semiconductor (such as InGaAs) between two wide bandgap semiconductors (e.g., GaAs and AlGaAs) and the carriers (two-dimension electron gas, 2DEG) in channel are populated by modulation doping.

GaAs devices are made as pHEMTs (pseudomorphic HEMTs) and mHEMTs (metamorphic HEMTs). The schematics of these devices are shown as Fig. 1. It is to note that the increase of indium content in the  $\text{In}_x\text{Ga}_{1-x}\text{As}$  channel enhances the saturation velocity and mobility of carriers, hence for given HEMT device features (for example, gate length), mHEMT has highest  $f_T$  (the gain of the device is measured as a function of frequency, it decreases with frequency and reaches to unity at  $f_T$ ), which is desirable for the device applications.

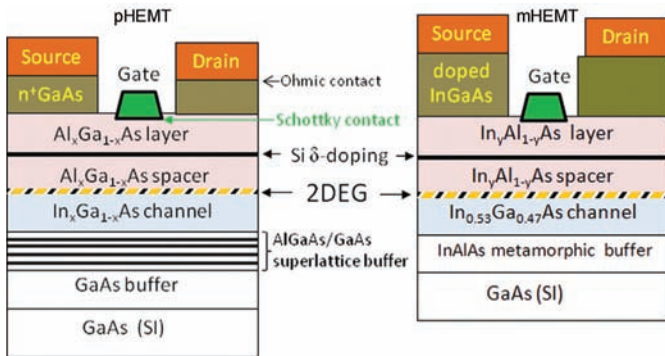


Figure 1. Schematics of pHEMT and mHEMT devices.

The pHEMT consists of  $\text{In}_x\text{Ga}_{1-x}\text{As}/\text{Al}_{0.24}\text{Ga}_{0.76}\text{As}$  device layers grown on semi-insulating GaAs buffer, which in turn is grown on GaAs substrate. In this case, the indium content ( $x$ ) of the channel layer is limited to about  $x = 0.2$  and its thickness is kept below critical thickness ( $\sim 10$  nm), which is composition-dependent. It is to be noted that the critical thickness corresponds to the thickness below which the lattice mismatch strain between the epilayer and the substrate is elastically accommodated and above which, the onset of misfit dislocations takes place.

In mHEMTs, high indium content ( $x \sim 0.53$ )  $\text{In}_x\text{Ga}_{1-x}\text{As}$  layer acts as the channel for two-dimensional electron gas (2DEG) conduction. To bridge this lattice mismatch ( $\sim 3.8$  per cent) with GaAs substrate, a specially designed  $\text{In}_x\text{Al}_{1-x}\text{As}$  buffer is grown on substrate with lattice parameter

grading by varying the indium content. In this case, misfit dislocations can originate and propagate as threading dislocations in the overgrown epilayers, if the growth conditions and the compositional grading of the metamorphic buffer are non-optimal. Ohmic metallisation (Au-Ge/Ni/Au layers), Schottky (gate, Pt/Au layers) metallisation, silicon nitride dielectric/passivation layers and interconnect metallisation are needed to make these HEMT structures as devices.

Authors carried out detailed electron microscopy studies of different device structures, such as  $\text{Al}_{0.24}\text{Ga}_{0.76}\text{As}/\text{GaAs}$  superlattice buffers, pHEMT device layers, mHEMT device layers, ohmic metallisation, gate metallisation, nichrome resistors and silicon nitride layers aimed at process optimisation. Representative TEM images of some of these device structures are as shown in Fig. 2. Detailed microstructural and property correlation studies on ohmic metallisation of HEMTs were conducted and the work is briefly described in later section.

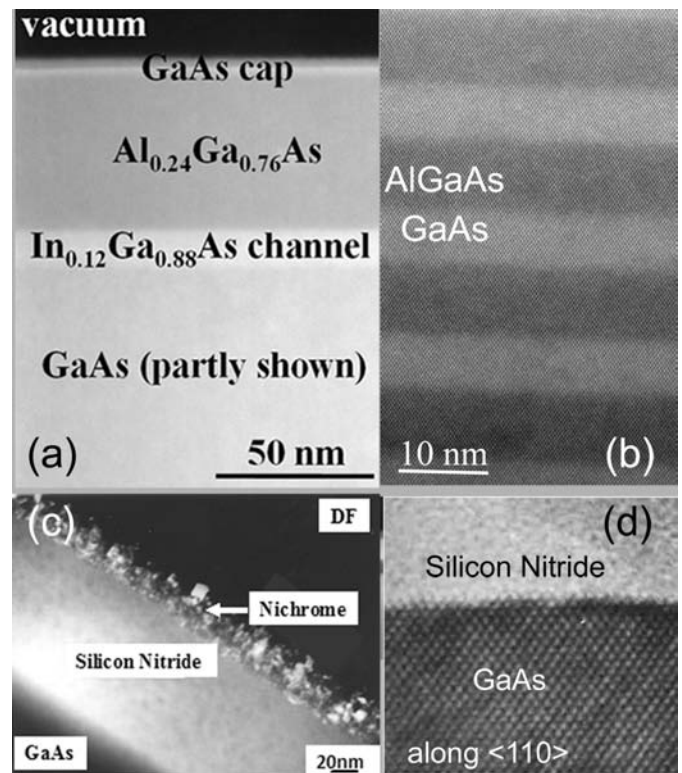


Figure 2. (a) and (b) show the cross-sectional view of pHEMT and AlGaAs/GaAs superlattice (partly) structures respectively, imaged by STEM-HAADF technique. Both structures (a-b) are grown by molecular beam epitaxy, (c) is the dark-field TEM image showing the cross-sectional view of nichrome thin film (for resistor applications) grown on silicon nitride coated GaAs substrate; the nichrome film is nanocrystalline with tunable temperature coefficient of resistance<sup>8,9</sup>, and (d) shows the interface of silicon nitride (amorphous) and GaAs (single crystalline), imaged by HRTEM technique.

### 2.1 Ohmic Metallisation of pHEMT and mHEMT Device Structures

The HEMT structures function as transistors after placing the Ohmic contacts and Schottky contacts (Fig. 1). The ohmic metal<sup>10</sup> acts as 'source' and 'drain' so that the carriers flow from

the former to the later through the channel. The Schottky metal contact functions as the gate and regulates the carrier flow.

The ohmic metallisation holds the key for the operation of HEMT device. A contact is said to be ohmic, if it obeys the Ohm's law, i.e., the current varies linearly with the potential difference across the contact. The Ohmic contact provides a low resistance path for current flow, both in and out of the channel. Low contact resistance, a smooth surface morphology with minimum roughness and high thermal stability are essential requirements.

In this work, Au-Ge/Ni/Au metal stack was used for ohmic metallisation of HEMT epilayers<sup>11-15</sup>. The rapid thermal annealing (RTA) promotes the intermixing of elements across the metal and semiconductor optimally so that low-contact resistance phases are formed at the interface. The TEM studies showed the formation of AuIn, Au-Ge and NiAs(Ge) phases, which are desirable. A correlation with electrical resistivity and electron microscopy study revealed that the typical RTA temperature ( $\sim 260$  °C) for the ohmic metallisation of mHEMT is much below the eutectic temperature of Au-Ge ( $\sim 360$  °C) whereas the optimally alloyed temperature ( $\sim 400$  °C) for its counterpart (i.e., pHEMT) is higher than this eutectic temperature. Also, the realised optimum contact resistance value of mHEMT is relatively higher vis-à-vis pHEMT.

In the ohmic metallisation of mHEMTs, the TEM studies showed a clear evidence for the outward-diffusion of indium and inward-diffusion of germanium and gold even at much lower RTA temperatures as compared to the eutectic temperature of Au-Ge layer. The presence of relatively higher indium content  $\text{In}_x\text{Ga}_{1-x}\text{As}$  channel layer in mHEMTs ( $x \sim 0.53$  in mHEMTs versus  $x \sim 0.12$  in pHEMTs) likely promotes the formation

of high concentration of indium vacancies, thus greater probability for intermixing at relatively lower temperatures vis-à-vis pHEMTs. The STEM-HAADF images (Figs. 3(b) and 3(c)) showed that there is interdiffusion of various elements across the interfaces. Upon RTA at  $260$  °C/45 s, the Au and Ge inward-diffusion resulted in a uniformly distributed  $100$  nm -  $200$  nm sized phases containing Au and Ge extending into the metamorphic buffer. These phases have coarsened in the over-alloyed sample (size  $\sim 1$   $\mu\text{m}$  at  $330$  °C) and penetrated deep inside the metamorphic buffer. NiAs phase was formed at the metal-semiconductor interface (Figs. 3(d)), which is very important for achieving a low contact resistance. However, indium diffused out all the way to the surface, reacted with Au in the ohmic metal stack and formed Au-In phase. As a result, the ohmic contacts are seriously degraded. The indium out diffusion even at low annealing temperatures ( $\sim 260$  °C/45 s) is possibly leading to indium vacancies in the epistucture. This appears to be the cause of in-diffusion of Ge and Au, up to and beyond the channel.

A careful *in-situ* SEM experiment (Fig. 4) carried out on ohmic metallisation of pHEMTs showed that the metal stack has a relatively fine grained surface in the as-deposited condition, however as it is heated, grains become more visible at  $100$  °C and at  $150$  °C. Very marginal grain growth is observed at  $200$  °C. Significant grain growth can be seen at  $300$  °C and  $350$  °C, and at  $400$  °C, grain deterioration starts by formation of pits. This study is in good agreement with plan-view SEM and cross-sectional TEM observations. It is likely that the indium content can play a role in the formation of indium vacancies in the channel layer.

We have also performed detailed microscopy studies of

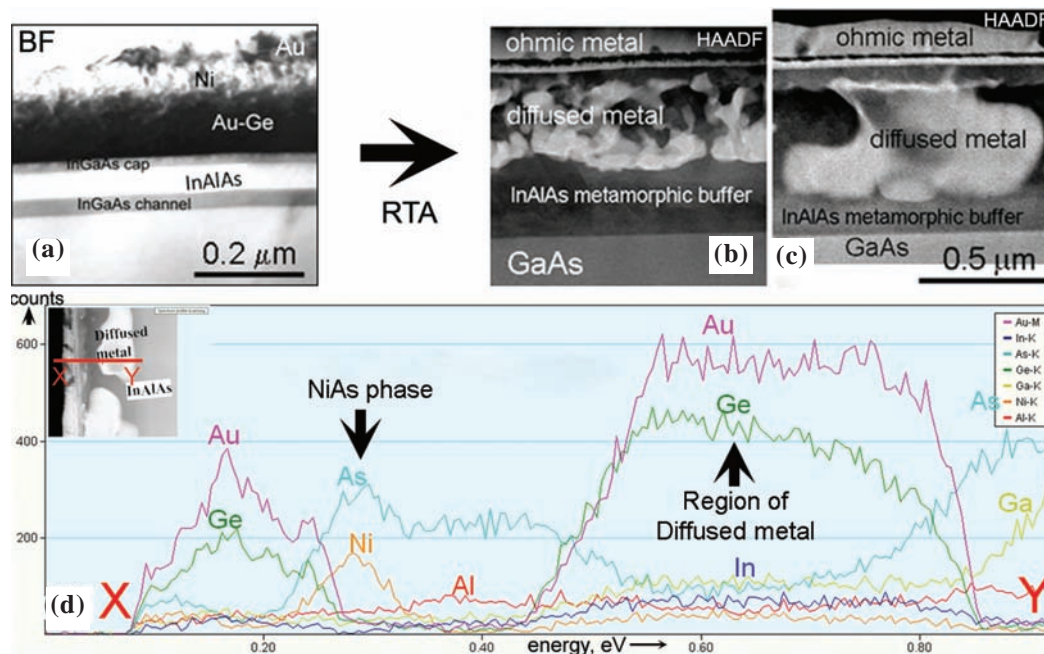


**Figure 3.** Ohmic metallisation of mHEMT device structure grown by MBE. (a) shows the cross-sectional TEM image of InGaAs/InAlAs epilayers over which Au-Ge/Ni/Au ohmic metal stack was deposited. This was subjected to rapid thermal annealing (RTA) at (b)  $260$  °C/45s and (c)  $330$  °C/45s. These images clearly show the interdiffusion of metal into the semiconductor layers. (d) shows the elemental profiles across the ohmic metal/HEMT layers [Inset in this figure is the reproduction of (c); the red line shows the probed region by STEM-EDS technique], confirming the Ni interdiffusion and forming NiAs layer at the metal-semiconductor interface. The diffused metal is very rich in Au and Ge elements.

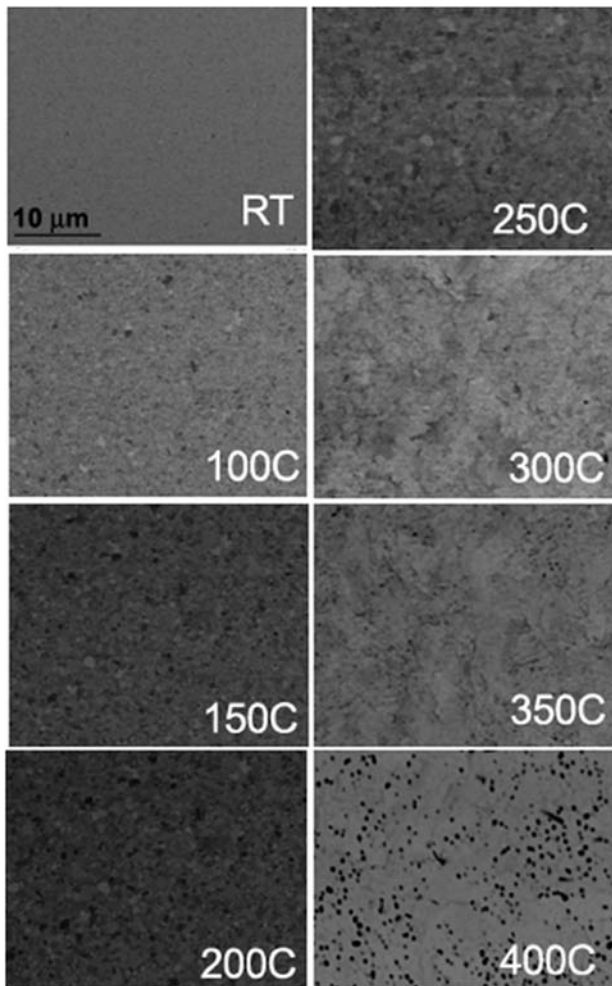


**Figure 4.** *In-situ* SEM study showing the evolution of microstructure of ohmic metal on pHEMT structure with temperature.

introducing platinum as a barrier layer between the ohmic metal stack and the semiconductor layers for enhancing the alloying temperature and improving the thermal stability. Though the optimum temperature was enhanced to 320 °C, only a marginal increase in the contact resistance was observed.

### 3. GaN HEMT DEVICE STRUCTURES

GaN HEMT technology is strategically important, due to high power (~10 times higher power vis-à-vis the conventional GaAs HEMTs) deliverability at microwave frequencies with high temperature operational capabilities. The GaN homoepitaxy is limited by the commercial availability of large-sized native substrates at an affordable cost; hence GaN epilayers are widely grown on silicon, sapphire and SiC. It is to be noted that the c-plane GaN has very large lattice mismatch with Si, sapphire and the associated strain relaxation manifests in GaN films in the form of

high density of microstructural defects, viz., misfit dislocations (MDs), threading dislocations (TDs), inversion domains (IDs), V-defects, etc. The electron microscopy methods, viz., weak-beam dark field imaging (WBDF), convergent beam electron diffraction (CBED), electron back scattered diffraction (EBSD), electron-energy loss spectroscopy and EDS methods are suitable for the detailed investigation of microstructural and compositional aspects<sup>16-25</sup> and the micro details are given in a detailed technical report<sup>26</sup>. These techniques have been applied for the study of these microstructural issues in GaN films. A representative EBSD study showing the crystalline misorientations of c-plane GaN is as shown in Fig. 5. The pole figure sheet (Fig. 5 (c)) clearly shows the non-basal plane GaN growth also.

A typical GaN HEMT structure consists of  $\text{Al}_x\text{Ga}_{1-x}\text{N}$  ( $x \sim 0.3$ , thickness  $\sim 20$  nm) / AlN spacer (thickness  $\sim 1$  nm) / GaN buffer (thickness  $\sim 3 \mu\text{m} - 5 \mu\text{m}$ ) layers grown on a substrate, with a suitable buffer or nucleation layer, by either MBE or MOCVD techniques. Due to spontaneous polarisation along the c-axis, a two-dimensional electron gas (2DEG) formation (without the necessity of doping in the wide-bandgap AlGaIn layer) takes place at the AlGaIn/GaN hetero-interface. The AlN layer placed at this interface acts as the 'spacer' layer. In this regard, the purity and thickness of this layer is very important. Our recent work<sup>27</sup> showed that the plasma-assisted MBE growth resulted in the growth of high pure AlN spacer layer without substantial incorporation of gallium, thus retaining its intrinsic band-gap property.

GaN growth on silicon is limited by high lattice mismatch and thermal mismatch. As a result, massive tensile strain builds up in the GaN film causing it to develop microcracks. This issue was addressed by employing a graded AlGaIn superlattice on AlN layer prior to GaN growth (Fig. 6(a)) and the resultant

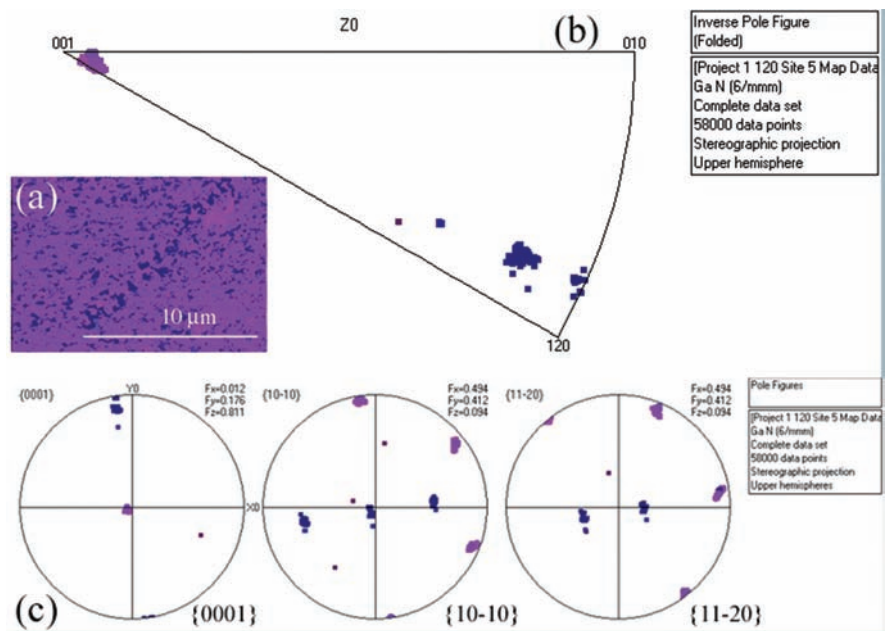


**Figure 5.** EBSD studies showing the crystalline misorientations in GaN film grown on c-plane sapphire with an AlN buffer layer by MOCVD technique: (a) shows the Euler map and corresponding inverse pole figure is shown as (b) and (c) is the pole figure sheet along different projections.

surface is smooth and predominantly free from microcracking (Fig. 6(b)) and with very narrow spread in the crystallite mosaicity (inset EBSD pole figure of Fig. 6(b)). Further, the AlGa<sub>0.7</sub>N/GaN epilayers are planar with a relatively smooth morphology (Fig. 6(c)).

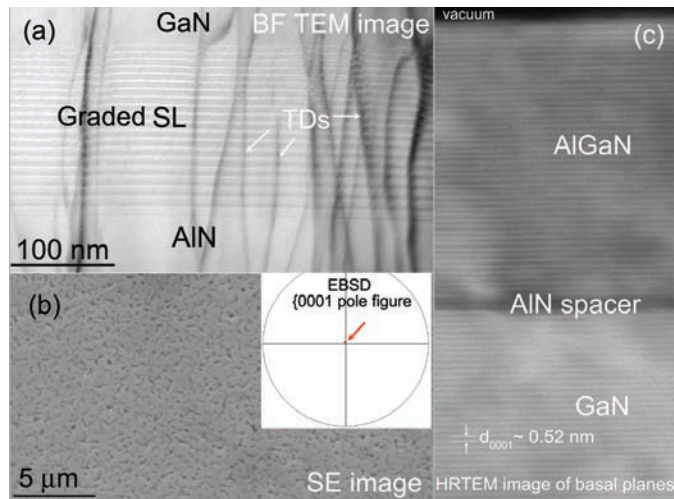


**Figure 6.** (a) Cross-sectional BF TEM image showing the AlGa<sub>0.7</sub>N graded superlattice (dark lines running across this structure are threading dislocations) employed for tensile strain management of GaN growth on Si (111), (b) The surface of AlGa<sub>0.7</sub>N/GaN HEMT structure grown on Si (111) is predominantly free from microcracks, and (c) The basal planes of the lattice showing a planar growth of the epitaxial layers.

### 3.1 Ohmic Metallisation of AlGa<sub>0.7</sub>N/GaN HEMTs

The AlGa<sub>0.7</sub>N/GaN HEMT technology finds high-power applications at microwave frequencies. For ohmic metallisation of GaN HEMTs, literature suggests the use of Ti-based contacts (*viz.*, Ti, Ti/Al, and Ti/Al/X/Au where X = Pt, Ni, Mo). It was shown that upon annealing at high-temperatures (at 600 °C or higher), Ti reacts with GaN forming TiN layer at the interface, which is desirable. The Ti/Al binary layer is found to be beneficial compared to the pure Ti layer due to its conductivity. However, Ti and Al can readily oxidise, hence Ti/Al binary layer needs to be passivated with Au layer. However, Au can diffuse during high-temperature annealing; therefore a barrier layer is kept across the Ti/Al and Au layers.

Hence, considering the above issues, a four-layer stack (Ti/Al/X/Au) metallisation has been used for the ohmic metallisation<sup>28,29</sup> of Al<sub>0.3</sub>Ga<sub>0.7</sub>N/GaN contact applications. Experiments were conducted by varying the thickness of Ti-layer and subjecting the contacts to a two-step rapid-thermal annealing (RTA) process, at 550 °C for 60 s and 740 °C for 30 s in succession. The investigations revealed:

- The surface of ohmic contacts exhibits a dendritic microstructure,
- The occurrence of Ti, Al, Ga elemental interdiffusion across the interfaces, and
- The formation of cubic TiN grains at the ohmic metal-AlGa<sub>0.7</sub>N interface.

The thickness of the Ti layer influences the dendrite size, surface roughness and contact resistance of the ohmic contacts,

(*viz.*, coarser dendrites with higher electrical resistivity with the increase of Ti layer thickness), as well as the interdiffusion of elements across the interfaces. Representative microstructures are shown as Fig. 7.

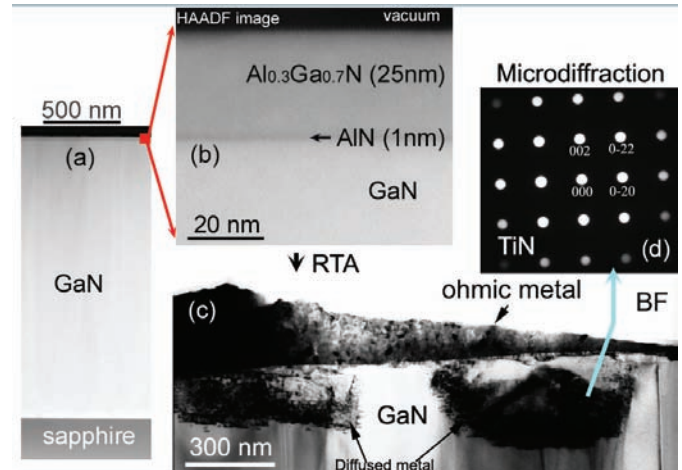


**Figure 7.** STEM-HAADF images as-deposited GaN HEMT structure: (a) at low-magnification, and (b) a close-up of the AlGa<sub>0.7</sub>N/AlN/GaN epilayers. Ti/Al/Ni/Au ohmic metal stack was deposited on this structure and subsequently alloyed by rapid-thermal annealing leading to interdiffusion of elements (c) and formation of TiN phase ((d), selected area diffraction pattern of TiN along <001>), which is desirable.

### 4. INFRARED DEVICE STRUCTURES

In recent years, antimonide based compound semiconductors (ABCS) are finding military and civilian applications for mid-wave infrared (MWIR) and long-wave infrared (LWIR) focal plane array (FPA) photodetectors. They exhibit a cubic lattice constant of about 6.1Å, hence they have been, together with InAs alloys, called as ‘6.1Å III-V family materials’. It is to be noted that the first generation IR detectors were made of lead salts (*viz.*, PbSe, PbTe), whereas the second generation detectors were based on the narrow bandgap semiconductors (mercury cadmium telluride, InSb) and GaAs/AlGaAs quantum well (QW)/InGaAs quantum dot (QD) IR photodetector technologies. The electrons follow laws of quantum physics in these quantum structures and exhibit quantum confinement effects. For example, In<sub>x</sub>Ga<sub>1-x</sub>As quantum dots (QDs) are the islands grown on GaAs by Stranski-Krastanov growth mode<sup>30</sup> and they are embedded in a relatively wider band gap semiconductor, such as GaAs, leading to the realisation of quantum confinement effects. These quantum dots are grown with in-plane self-organisation as well as with vertically aligned multilayers<sup>31-33</sup> (Fig. 8). The MCT detectors have high quantum efficiency (QE), however limited by very narrow compositional window for growth, microstructural defects, high cost Cadmium Zinc Telluride (CZT) substrates and those grown on Silicon are limited to MWIR band applications. The InSb system is unsuitable for LWIR applications. On the other hand, GaAs/AlGaAs quantum well infrared photodetectors (QWIPs) exhibit relatively low QE due to insensitivity to surface-normal incident radiation. Due to these shortcomings, the new generation materials, *viz.*, InAs/(In,Ga)Sb system,

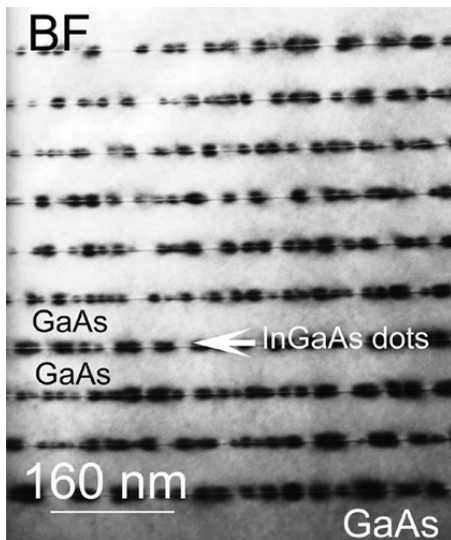


**Figure 8.** In GaAs multilayered quantum dots grown on (001) GaAs substrate by MBE.

characterised by ‘misaligned’ Type - II band alignment (popularly known as Type II strained layer superlattice or T2SL), are currently in focus for FPA applications. This class of materials has the desirable features of high spatial uniformity, high resolution, multi-band IR detection, low-noise and high temperature operational capability. Also, the effective bandgap can be tailored over a wide range, by varying the thickness of epilayers of constituent materials (GaSb and InAs).

Ideally, the GaSb-based IR device structures should be grown *homoepitaxially*, however GaAs substrates are in use due to lower cost and availability in large diameter. In this context, a major issue is that the GaSb has a large lattice mismatch ( $\sim 7.8$  per cent) with the GaAs (refer Fig. 9(a)) for [001] growth; GaSb on GaAs experiences compressive strain and the strain relaxation results in the misfit dislocations (MDs). Generation of  $60^\circ$  MDs (dislocation line direction and its Burgers vector are at  $60^\circ$ , viz., for (001) growth, the dislocation having line direction of  $[1-10]$  and Burgers vector  $\frac{1}{2}[101]$  or  $\frac{1}{2}[01-1]$ ) creates threading dislocations (TDs), which degrade the overgrown device layers. Hence, it is important to restrict them. Their formation can be minimised by creating a network of periodic Lomer dislocations or  $90^\circ$  MDs (dislocation’s line direction and Burgers vector are at  $90^\circ$ ) along orthogonal  $\langle 110 \rangle$  directions and contained in the (001) interface. This is known as interfacial misfit (IMF) array method. It is to be noted that the relaxation kinetics favor  $60^\circ$  MD as this type of dislocation can guide to the surface, however  $90^\circ$  MD can very effectively relax the mismatch strain (twice as efficient as compared to  $60^\circ$  MD). The strain relaxation by forming Lomer dislocations produces high quality GaSb template growth over GaAs. The IMF method involves a particular arrangement of the antimony atoms to the Ga-surface of GaAs, which is achieved by specific growth conditions.

In our recent study, GaSb thin films were grown (a) directly and (b) by IMF method on (001) epi-ready GaAs substrates by molecular beam epitaxy (MBE). Detailed microstructural characteristics (surface morphology and microstructural defects) were determined by SEM, TEM, and

AFM techniques. The studies revealed that the IMF method enabled the growth of relaxed GaSb with minimal creation of residual TDs (refer Fig. 9, representative cross-sectional TEM images of GaSb films).

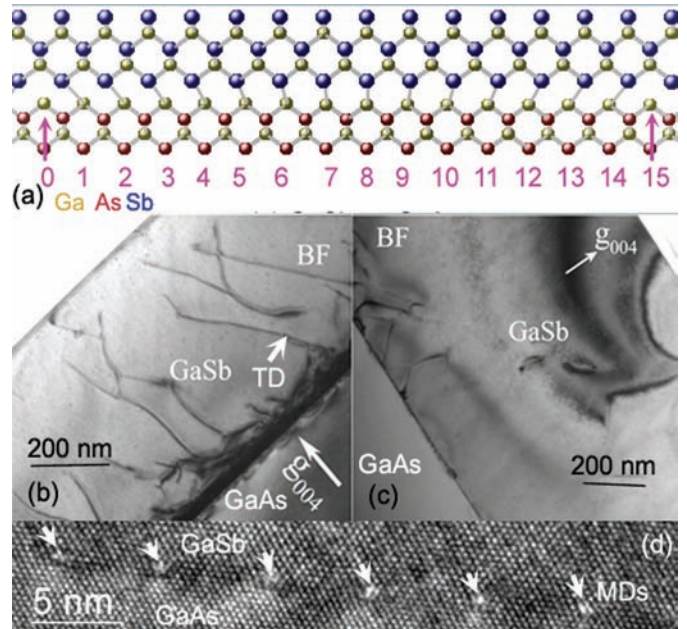


**Figure 9.** (a) Schematic showing the projection of GaSb and GaAs lattices along  $\langle 110 \rangle$  orientation (considering the respective equilibrium cubic lattice parameters as  $6.09 \text{ \AA}$  and  $5.65 \text{ \AA}$ ); the crystals are completely in registry at position 8 and the resultant misfit dislocations are at positions 0 and 15, (b) Cross-sectional image showing high TD density for direct growth of GaSb on GaAs, (c) significant TD reduction by the IMF growth of GaSb on GaAs, which is due to the formation of highly periodic array of  $90^\circ$  misfit dislocations at the interface, shown with arrows in (d) : HRTEM image.

## 5. NANOSTRUCTURES

Nanowires are useful for sensor applications. TEM studies are useful for the detailed study of microstructural defects, epitaxy and polarity of nanowires<sup>34,35</sup>. We have investigated the self-induced GaN nanowire (NW) growth on Si (211) substrate by plasma-assisted MBE as well as InAs nanowires growth by MBE techniques respectively. The detailed electron microscopy studies<sup>35</sup> showed that the GaN NWs grew on the nitridated Si substrate epitaxially with their  $\{0001\}$  basal planes parallel to the  $\{111\}$  planes of Si. The Si (211) is a stepped surface with  $\{111\}$  terraces and  $\{001\}$  ledges and the GaN NWs grew on the terraces preferentially. Since the ideal Si (211) surface has an angle of about  $20^\circ$  with the Si (111) planes, the grown NWs are inclined at this angle. Also, the nitridated region at the interface between the Si substrate and GaN NW is amorphous.

A representative electron microscopy study of InAs NWs grown on (111) silicon substrate is shown in Fig. 10. A 30 nm thick oxide ( $\text{SiO}_2$ ) layer was grown on Si, which was subsequently thinned to about 2 nm by chemical etching. The self assembled nanowires were grown without use of any catalyst. The substrate temperature and V/III ratio were

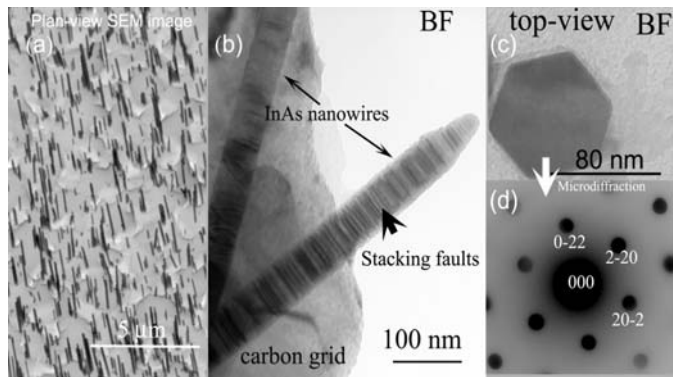


**Figure 10. Electron microscopy images of InAs nanowires: (a) plan-view SEM image showing the distribution of InAs nanowires, (b) TEM image showing the morphology of NWs, and (c) cross-section of one of the NWs and the corresponding microdiffraction pattern along  $\langle 110 \rangle$  orientation.**

kept at 450 °C and 200 °C, respectively. The NWs exhibited hexagonal cross-section having a side length of about 60 nm and with faceted tips. Also, the NWs have a high density of stacking faults on  $\{111\}$  planes.

## 6. ADVANCED MICROSCOPY TECHNIQUES

### 6.1 Convergent Beam Electron Diffraction

In the conventional TEM techniques, a nearly parallel electron beam interacts with the TEM specimen. On the other hand, in the CBED technique, the electron beam is made as a convergent beam. As a result, the diffraction spots appearing in a typical electron diffraction pattern appear as disks. Due to the dynamical diffraction effects, the Ewald sphere intersecting with the reflections at the higher order Laue zones (HOLZ) can result in the appearance of sharp ‘deficit’ lines (known as HOLZ lines) in the transmitted (000) disk. The positions of these lines are dependent upon the orientation, composition and lattice parameters of the specimen and the operating voltage of TEM. Hence, one of these parameters can be determined if others are known, by performing the HOLZ line simulations. One of the advantages of the CBED technique is its high spatial resolution.

We have established the methodologies for the determination of the voltage of TEM operated at 200 kV<sup>36</sup> and 250 kV<sup>37</sup> with detection sensitivity of the order of 100 V. For illustration, Fig. 11 which shows the positions of the HOLZ lines, observed for silicon along  $[37\ 37\ 4]$  orientation at various operating voltages of the TEM. The positions of intersections, formed by HOLZ lines 1 and 2, and 3 and 4, merges at 199.1 kV, hence this can be used for calibration of the voltage of TEM<sup>36</sup>.

Also, a methodology has been established for the quantitative study of lattice distortions (changes in the lattice spacings of the order of  $2 \times 10^{-4}$  nm) in GaAs and GaN films; and composition of GaAs based epilayers<sup>5,6,38</sup>.

It is to be noted that the identification of suitable HOLZ lines with desired sensitivity requires an elaborate exercise, involving especially the analysis of several HOLZ line patterns calculated by dynamical diffraction effects with advanced

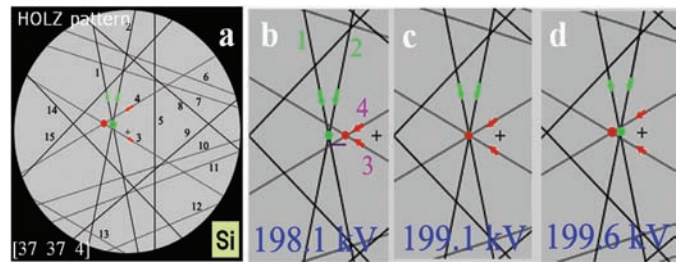


**Figure 11. HOLZ lines (simulated by JEMS software) in the transmitted disc of Silicon single crystal along  $[37\ 37\ 4]$  orientation for various TEM voltages.**

software tools such as JEMS<sup>39</sup>. In this context, the HANSIS program (software tool) is useful for the automated analysis of HOLZ lines by simultaneous evaluation of multiple HOLZ patterns<sup>40</sup>.

The zincblende/wurtzite crystals exhibit polarity along  $\langle 111 \rangle$  and  $\langle 0001 \rangle$  directions respectively. The polarity is an important property, viz., surface of N-polar GaN can be wet-chemically etched faster than its counterpart (Ga-polar GaN). In this context, the intensity distribution inside the disks of a low-index zone CBED pattern can be useful to determine the crystal polarity. For example, ‘wurtzite’ GaN crystal is polar along  $\langle 0001 \rangle$  direction and its polarity can be determined using the CBED technique. For illustration, the polarity model assumed for the GaN crystal Fig. 12(a) and the corresponding simulated CBED pattern along  $[10\ -10]$  zone axis are shown as Fig. 12(b). Here, the intensities of 0002 and 000-2 disks are dissimilar and lack mirror symmetry due to the non-centrosymmetry of the GaN crystal about the  $[0001]$  direction. Thus, the polarity of the GaN epilayer can be known by relating the surface normal to the disks.

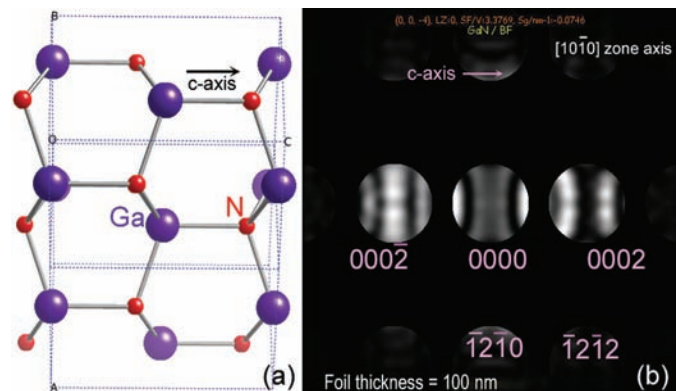


**Figure 12. (a) Wurtzite GaN crystal. The  $[0001]$  c-direction marks the direction of Ga-N bond direction. The CBED pattern along  $\langle 10\ -10 \rangle$  zone axis, simulated by JEMS software<sup>39</sup> under dynamical diffraction conditions. Due to the lack of centre of symmetry, the intensities of 0002 and 000-2 discs are dissimilar. This information can be utilised for identification of polarity of the GaN crystal.**

### 6.2 Aberration-corrected TEM

In the early 1980’s, high voltage electron microscopy ( $\sim 1$  MV) was primarily utilised to resolve the lattice planes of the crystalline materials. In this case, the point resolution was

$\sim 1.6 \text{ \AA}$  and achieving below  $1 \text{ \AA}$  was a dream. This was primarily due to the aberrations (spherical aberration,  $C_s$  and chromatic aberration,  $C_c$ ), which could not be corrected due to the cylindrical symmetric electromagnetic fields originating from the lens system of TEM. However, since 1990's, there is a conceptual change and with the introduction of new ideas and instrumentation (high brightness gun, monochromator, spherical/chromatic aberration correctors, mechanical and electrical stabilities), the  $1 \text{ \AA}$  barrier was broken in both scanning transmission electron microscopy (STEM) and high-resolution transmission electron microscopy (HRTEM) modes of operation in mid-voltage ( $\sim 200 \text{ kV} - 300 \text{ kV}$ ) range<sup>41</sup>. For example, Ga-As dumbbells of GaAs are resolved in Fig. 16. Also, it is realised with relatively large gap pole-pieces so that high specimen tilt and in-situ experimentations are possible. These developments have opened great opportunities for the microstructural analysis of semiconductor heterostructures. For example, the atomic steps at the AlGaIn/AlN/GaN interfacial region as shown in Fig. 13.

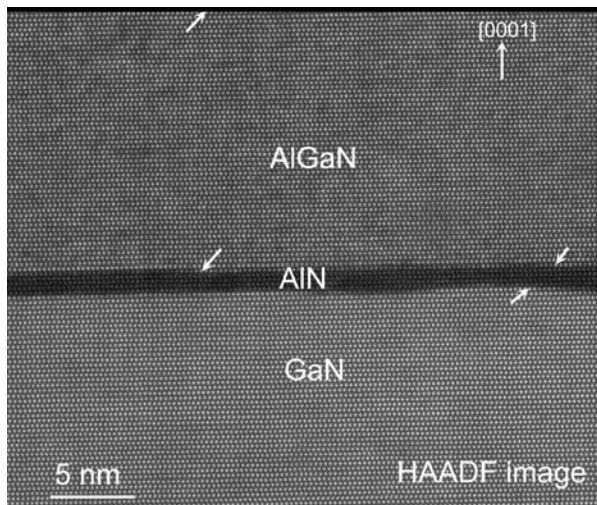


**Figure 13. STEM-HAADF image showing the GaN/AlN/AlGaIn interfaces. Atomic steps are noticed at the arrow-marked regions.**

### 6.3 Spectroscopy: EDS and EELS

There are significant improvements in the instrumentation of electron-energy loss spectroscopy (EELS) and energy-dispersive X-ray spectroscopy (EDS) coupled as accessories to the TEM as the compositional tools. For example, the EELS spectral resolution has been improved to  $\sim 100 \text{ meV}$  or better. As a result, ample opportunities are present to study electron-loss near edge structure (ELNES) and plasmonics. Similarly, the modern EDS systems are built with large-sized integrated multiple detectors so that quantitative compositional studies/X-ray elemental maps can be performed with improved accuracy in a short time. We have been employing EELS and EDS techniques to study a variety of electronic materials. For illustration, a representative x-ray line scan for the AuGe/Ni/Au ohmic metallisation of mHEMTs is shown in Fig. 3(d).

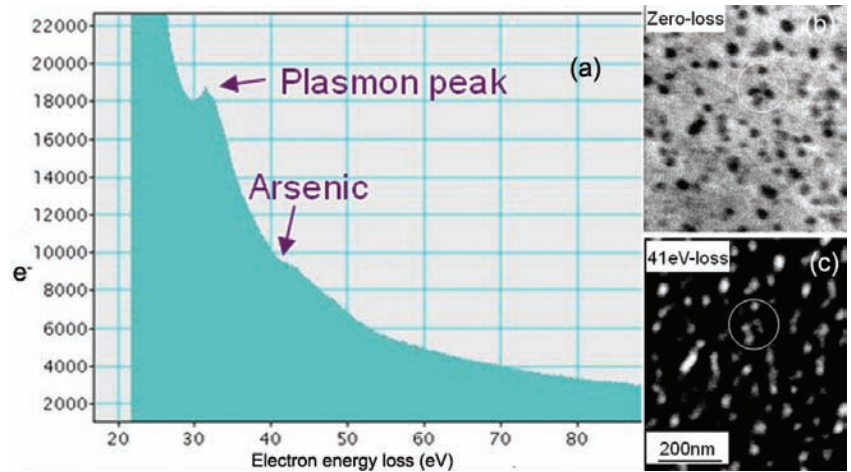


**Figure 14. EELS study of annealed LT GaAs. (a) shows EELS spectrum of the specimen (b). The electron energy-loss peak at 41 eV corresponds to As. (c) Energy-filtered TEM (EFTEM) mapping at 41 eV. The bright contrast features have a one-to-one relationship with the dark contrast features in (b), thus confirming them to be arsenic precipitates.**

Also, mapping of arsenic precipitates in low-temperature grown GaAs (LT GaAs<sup>42</sup>), by EELS based energy-filtered TEM (EFTEM) technique, is as shown in Fig. 14. It is to be noted that GaAs grown at low-temperature under arsenic over-pressure (LT GaAs) by MBE technique is non-stoichiometric. It contains small concentration of excess arsenic as point defects, which evolve as arsenic precipitates upon annealing. This material finds applications as high-resistive buffers.

### 6.4 Quantitative HAADF Study of Interfaces

Recent years witnessed the advancements in quantitative electron microscopy techniques based on image analysis, for example, digital analysis of lattice images (DALI), geometrical phase analysis (GPA), peak-pair analysis (PPA), Column-ratio mapping, STEM-SIM etc., which resulted in the quantification of strain across heterointerfaces from HRTEM images, interfacial abruptness/roughness and the composition of individual epilayers from the HAADF images. Representative computational facilities in DMRL for the quantitative analysis of HRTEM images are briefly described as follows.

#### 6.4.1 DALI

Digital analysis of lattice images (DALI) software<sup>43</sup> takes digital HRTEM image as input and can provide spatial variation of strain and composition in heteroepitaxial structures. The compositional variations across multilayers in the heterostructures result in varying lattice spacings which is affected anisotropically in the growth direction and the in-plane direction because of the constraint imposed by the underlying lattice on which the structure is grown. We have recently analysed HRTEM images of AlGaAs/InGaAs/GaAs pHEMT structure for quantifying the strain and composition of the InGaAs channel and the details are given in literature<sup>7</sup>.

For illustration, in the AlGaIn/AlN/GaN multilayered HEMT structure (Fig. 15(a)), the bulk lattice spacing of AlN is smaller than that of GaN. As the AlN grows in registry with the underlying (0001) GaN lattice, it is constrained to assume the

lattice spacing of GaN in directions perpendicular to the growth direction (Fig. 15(c)) with a resulting biaxial tensile stress on the growth plane. This constraint leads to a contraction of the lattice along the growth direction (Fig. 15(b)). DALI performs the quantitative analysis by comparing the lattice distances of the actual structure with reference to those of a reference lattice. The latter is generated on the basis of a selected region in the undistorted (strain-free) area of the digital HRTEM image. Figure 15 shows that the lattice spacings of AlN and GaN in the in-plane directions are similar suggesting that AlN is completely strained. However, along the growth direction, the lattice spacings of the AlN region are about 95 per cent that GaN, which amounts to effective *c*-parameter to be 0.49258 nm or a strain of -1.08 % (with reference to bulk *c*-lattice parameter of 0.49795 nm of AlN). It is possible to analyse the strain and composition of non-stoichiometric layers too using analytical expressions for the extreme cases of thin and thick TEM foils, as described for the case of a pHEMT structure published elsewhere<sup>7</sup>.

#### 6.4.1 Column-ratio Mapping

As explained earlier, high resolution aberration corrected electron micrograph can resolve spatial features at sub-Angstrom levels. In a III-V compound semiconductor, the atomic columns corresponding to the third and fifth groups appear as dumbbells as shown in the schematic (Fig. 16(b)). Within each dumbbell, STEM-HAADF image contrast varies based on the atomic number of the element, which is called as Z-contrast (i.e., columns corresponding to the third group elements are less intense compared to those corresponding to the fifth group). The intensities of the columns can be digitally processed and after removing the contribution from the background, a map of the intensities due to the group III

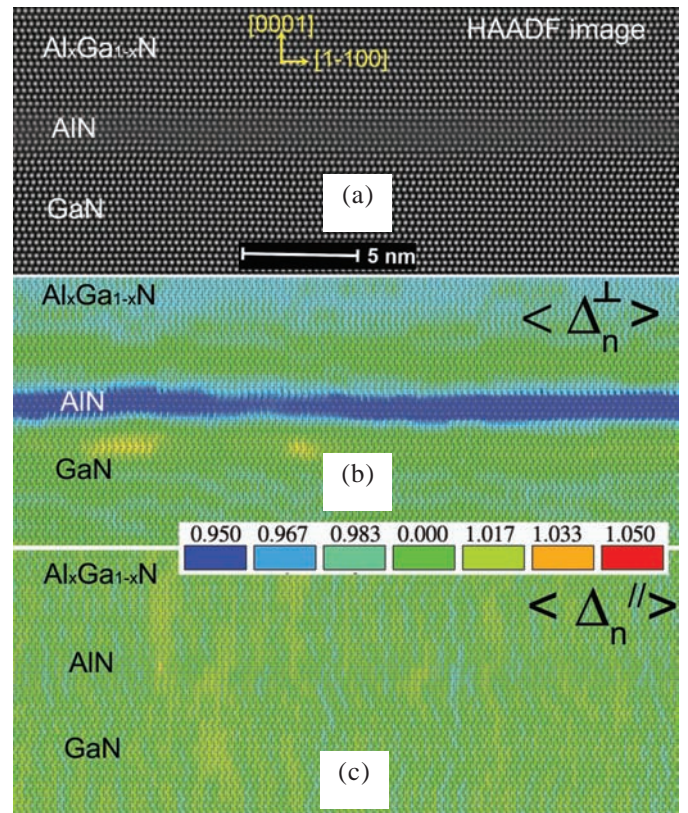


**Figure 15.** (a) STEM-HAADF image of AlGa<sub>1-x</sub>N/AlN/GaN HEMT structure along <math>\langle 11\bar{2}0 \rangle</math> zone axis. (b) and (c) represent the relative changes in lattice spacings perpendicular and parallel to the heterointerfaces, (i.e., parallel and perpendicular to the [0001] growth directions) respectively. The GaN lattice in (a) is considered as reference for the calculation of lattice spacings.

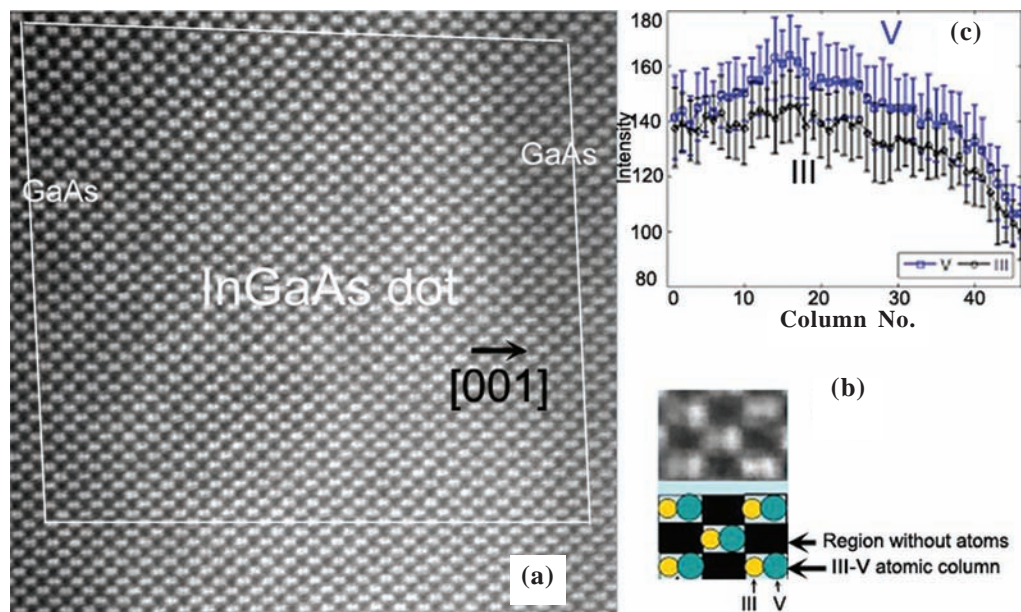


**Figure 16.** (a) <math>\langle 110 \rangle</math> STEM-HAADF image showing In<sub>x</sub>Ga<sub>1-x</sub>As quantum dot embedded in GaAs with the region analysed shown by a white rectangle, (b) experimental image along with a schematic showing the group III and group V atoms with the intensity represented by choosing different diameters and colors for them. The background intensity is obtained from region represented by black rectangles, (c) the analysed average intensities due to group III and group V atomic columns after background subtraction.

and group V columns can be mapped<sup>44</sup>. Figure 16(c) shows the average intensities of these columns (averaged over the rows within the selected region) for an InGaAs quantum dot (Fig. 16(a)). Using this technique, it is possible to analyse the quality of the interface in the device structures wherein diffusion of species takes place as a result of chemical potential gradients.

## 7. SUMMARY

This paper gives an overview of our efforts in establishing various advanced electron microscopy techniques for the microstructural and compositional characterisation of III-V compound semiconductor thin films. The techniques included SEM and TEM based imaging and diffraction techniques, such as orientation imaging, high-resolution transmission electron microscopy, Scanning transmission electron microscopy based high-angle annular dark field imaging, energy-dispersive x-ray spectroscopy and electron energy loss spectroscopy. The application areas presented shows the utility of these techniques for the investigation of MBE grown and MOCVD grown GaAs, GaSb and GaN nanostructures, in the form of thin films and nanowires.

## REFERENCES

- Howes, M.J. & Morgan, D.V. Gallium Arsenide: Materials, devices, and circuits. Wiley Series in Solidstate Devices and Circuits. 1985, Chichester, John Wiley and Sons.
- Phillips, Jamie. Evaluation of the fundamental properties of quantum dot infrared detectors. *J. Appl. Phys.*, 2002, **91**(7), 4590-4594. doi: 10.1063/1.1455130
- Sridhara Rao, D.V.; Muraleedharan, K.; Bysakh, S.; Balamuralikrishnan, R.; Nandy, T.K.; Muralidharan, R.; Srinivasan, T.; Mishra, P.; Sen, P.; Vankar, V.D. & Banerjee, D. Characterisation of GaAs based semiconductor device structures. *In* Frontiers in Design of Materials, 2007, CRC Press, Taylor & Francis.
- Sridhara Rao, D.V.; Muraleedharan, K. & Humphreys C. J. TEM specimen preparation techniques. *In* Microscopy: Science, Technology, Applications and Education, 2011, Formatex, Spain, 1232-1244.
- Sridhara Rao, D.V.; McLaughlin, K.; Kappers, M.J. & Humphreys, C. J. Lattice distortions in GaN on sapphire using the CBED-HOLZ technique, *Ultramicroscopy*, 2009, **109**(10), 1250-1255. doi: 10.1016/j.ultramic.2009.05.018
- Sridhara Rao, D.V.; Muraleedharan, K.; Balamuralikrishnan, R.; Banerjee, D.; Holec, D.; Kappers, M.J. & Humphreys, C.J. Determination of the lattice parameters and composition of III-V semiconductor thin films using the CBED-HOLZ technique. *In* Proceedings of International Workshop on Physics of Semiconductor Devices. New Delhi, 2009, 134-139.
- Sridhara Rao, D.V.; Sankarasubramanian, R.; Muraleedharan, K.; Mehrtens, T.; Rosenauer, A. & Banerjee, D. Quantitative strain and compositional studies of  $\text{In}_x\text{Ga}_{1-x}\text{As}$  epilayer in a GaAs-based pHEMT Device Structure by TEM Techniques. *Microscopy Microanalysis*, 2014, **20**, 1262-1270. doi: 10.1017/S1431927614000762
- Sridhara Rao, D.V.; Muraleedharan, K.; Vinayak, S. & Vyas, H.P. TEM Characterization of nichrome thin films. *In* 11<sup>th</sup> International Workshop on the Physics of Semiconductor Devices, Proceedings of SPIE - the International Society for Optical Engineering, 2002, **2**, 1190-92.
- Vinayak, S.; Vyas, H.P.; Muraleedharan, K. & Vankar, V.D. Ni-Cr thin film resistor fabrication for GaAs monolithic microwave integrated circuits. *Thin Solid Films*, 2006, **514**(1-2), 52-57. doi: 10.1016/j.tsf.2006.02.025
- Braslau, N; Ohmic contacts to GaAs, *Thin Solid films*, 1983, **104**, 391. doi: 10.1016/0040-6090(83)90581-3
- Sai Saravanan, G.; Mahadeva Bhat, K.; Dhamodaran, S.; Pathak, A.P.; Muralidharan, R., Vyas, H.P.; Sridhara Rao, D.V.; Balamuralikrishnan, R. & Muraleedharan, K. Evolution of surface morphology of alloyed AuGe/Ni/Au ohmic contacts to GaAs microwave FETs. *Mat. Sci. Semicon. Proc.*, 2015, **30**, 62-74. doi: 10.1016/j.mssp.2014.09.041
- Sai Saravanan, G.; Mahadeva Bhat, K.; Muraleedharan, K.; Vyas, H.P.; Muralidharan, R. & Pathak, A.P. Ohmic contacts to pseudomorphic HEMTs with low contact resistance due to enhanced Ge penetration through AlGaAs layers. *Semicon. Sci. Technol.*, 2008, **23**, 025019. doi: 10.1088/0268-1242/23/2/025019
- Mahadev Bhat, K. Study on ohmic contact formation, selective gate recessing and gate recess structure engineering in high electron mobility transistors. IIT, Madras, Chennai. 2013, PhD Thesis.
- Mahadeva Bhat, K.; Sridhara Rao, D.V.; Sai Saravanan, G.; Vyas, H. P.; Badnikar, S. L.; Muralidharan, R.; Jain, M.K. & Subrahmanyam, A. Electron microscopy study of AuGe/Ni/Au ohmic contacts to GaAs mHEMT structure. *In* EMSI Golden Jubilee conference, Hyderabad, July 6-8, 2011, 167-169.
- Mahadeva Bhat, K.; Saptarshi Mandal; Saptarshi Pathak; Sai Saravanan, G.; Sridhar. Ch.; Badnikar, S.L.; Vyas, H.P.; Muralidharan, R.; Jain, M.K.; & Subrahmanyam, A. Gate recess structure engineering using silicon-nitride assisted process for increased breakdown voltage in pseudomorphic HEMTs, *Semicon. Sci. Technol.*, 2012, **27**(11), 115013. doi: 10.1088/0268-1242/27/11/115013
- Kappers M.J.; Hollander J.L.; Johnston C.F.; McAleese C.; Sridhara Rao D.V.; Sanchez A.M.; Humphreys, C.J.; Badcock, T.J. & Dawson, P. Properties of non-polar a-plane GaN/AlGaIn quantum wells. *J. Crystal Growth*, 2008, **310**, 4983-4986. doi: 10.1016/j.jcrysgro.2008.08.048
- Badcock T.J.; Dawson, P.; Kappers, M.J., McAleese, C.; Hollander, J.L.; Johnston, C.F.; Sridhara Rao, D.V.; Sanchez, A.M. & Humphreys C.J. Optical polarization anisotropy of a-plane GaN/AlGaIn multiple quantum well structures grown on r-plane sapphire substrates. *J. Appl. Phys.*, 2009, **105**, 123112. doi: 10.1063/1.3156688
- Moram, M. A.; Ghedia, C. S.; Sridhara Rao, D.V.; Barnard J.S.; Zhang, Y.; Kappers, M.J. & Humphreys C.J. On the origin of threading dislocations in GaN films. *J. Appl. Phys.*, 2009, **106**, 073513. doi: 10.1063/1.3225920
- Ashraf, H.; Sridhara Rao, D.V.; Gogova, D.; Siche, D.; Fornari, R.; Humphreys, C.J. & Hageman, P.R. Reduction

- of the dislocation density in HVPE-grown GaN epi-layers by an in situ SiN<sub>x</sub> treatment. *J. Crystal Growth*, 2010, **312**(4), 595-600. doi: 10.1016/j.jcrysgro.2009.11.043
20. Kappers, M.J.; Moram, M.A.; Sridhara Rao, D.V.; McAleese, C. & Humphreys, C.J. Low dislocation density GaN growth on high-temperature AlN buffer layers on (0001) sapphire. *J. Crystal Growth*, 2010, **312**(3), 363-367. doi: 10.1016/j.jcrysgro.2009.11.014
  21. Sridhara Rao, D.V.; Beanland, R.; Kappers, M.J.; Zhu, D. & Humphreys, C.J. Lattice distortions in GaN thin films on (0001) sapphire. *J. Phys.: Conf. Ser.*, 2010, **209**, 012022. doi: 10.1088/1742-6596/209/1/012022
  22. Lewis Z.Y, Liu; Sridhara Rao, D.V.; Kappers, M.J.; Humphreys, C.J. & Geiger, D. Basal-plane stacking faults in Non-polar GaN studied by off-axis electron holography. *J. Phys.: Conf. Ser.*, 2010, **209**, 012012. doi: 10.1088/1742-6596/209/1/012012
  23. Zhu, T.; Moram, M.A.; Sridhara Rao, D.V.; Li, H.; Kappers, M. J. & Oliver, R. A. The impact of ScO<sub>x</sub>N<sub>y</sub> interlayers on unintentional doping and threading dislocations in GaN. *J. Phys.: Conf. Ser.*, 2010, **209**, 012067. doi: 10.1088/1742-6596/209/1/012067
  24. Holec, D.; Zhang, Y.; Sridhara Rao, D.V.; Kappers, M. J.; McAleese, C. & Humphreys, C. J. Equilibrium critical thickness for misfit dislocations in III-nitrides. *J. Appl. Phys.*, 2008, **104**, 123514. doi: 10.1063/1.3033553
  25. Pramanik, P.; Sen, S.; Singh, C.; Roy, A.S.; Das, A.; Sen, S.; Bhattacharyya, A.; Kumar, D. & Sridhara Rao, D.V. Controlling the compositional inhomogeneities in Al<sub>x</sub>Ga<sub>1-x</sub>N/Al<sub>y</sub>Ga<sub>1-y</sub>N MQWs grown by PA-MBE: Effect on luminescence properties. *J. Crystal Growth*, 2016, **439**, 60-65. doi: 10.1016/j.jcrysgro.2016.01.004
  26. Sridhara Rao, D.V. Microscopy techniques for microstructural and compositional characterisation of GaN based thin films. DMRL Technical Report, Report No. DRDO-DMRL-EMG-084-2015
  27. Sridhara Rao, D.V.; Jain, A.; Lamba, S.; Muraleedharan, K. & Muralidharan, R. Electron microscopy investigations of purity of AlN interlayer in Al<sub>x</sub>Ga<sub>1-x</sub>N/GaN heterostructures grown by plasma assisted molecular beam epitaxy. *Appl. Phys. Lett.*, 2013, **102**, 191604. doi: 10.1063/1.4805027
  28. Sridhara Rao, D.V.; Kumar, D.; Vinayak, S; Muralidharan, R; Kappers, M.J; Humphreys, C.J & Muraleedharan, K. TEM studies of Ti/Al/Ni/Au ohmic contacts to Al<sub>0.3</sub>Ga<sub>0.7</sub>N/GaN HEMTs. In EMSI Golden Jubilee conference, Hyderabad, July 6-8, 2011, 164-166.
  29. Mahajan, S.S. ; Dhaul, A.; Laishram, R.; Kapoor, S.; Vinayak, S. & Sehgal, B.K. Micro-structural evaluation of Ti/Al/Ni/Au ohmic contacts with different Ti/Al thicknesses in AlGaIn/GaN HEMTs. *Mat. Sci. Eng. B*, 2014, **183**, 47–53. doi: 10.1016/j.mseb.2013.12.005
  30. Bimberg, D.; Grundmann, M. & Ledentsov, N.N. Quantum dot heterostructures. John Wiley & Sons, Chichester, 1999
  31. Srinivasan, T.; Singh, S.N.; Mehta, S.K.; Muralidharan, R.; Sridhara Rao, D.V.; Balamuralikrishnan, R. & Muraleedharan, K. Structure and photoluminescence characteristics of molecular beam epitaxially grown vertically aligned In<sub>0.33</sub>Ga<sub>0.67</sub>As/GaAs quantum dots. *J. Crystal Growth*, 2005, **280**, 378-384. doi: 10.1016/j.jcrysgro.2005.04.010
  32. Sridhara Rao, D.V.; Muraleedharan, K.; Balamuralikrishnan, R.; Muralidharan, R.; Srinivasan, T. & Banerjee, D. TEM studies of In<sub>0.33</sub>Ga<sub>0.67</sub>As multilayered quantum dots. *J. Phys.: Conf. Ser.*, 2010, **209**, 012037. doi: 10.1088/1742-6596/209/1/012037
  33. Srinivasan, T.; Mishra, P.; Jangir S.K.; Raman, R.; Sridhara Rao, D.V.; Rawal D.S. & Muralidharan, R. Molecular beam epitaxy growth and characterisation of silicon – Doped InAs dot in a well quantum dot infrared photo detector (DWELL-QDIP). *Infrared Phy. Technol.*, 2015, **70**, 6-11. doi: 10.1016/j.infrared.2014.12.001
  34. Rathore, N.; Sridhara Rao, D.V. & Shaibal K, Sarkar. Growth of a polarity controlled ZnO nanorod array on a glass/FTO substrate by chemical bath deposition, *RSC Advances*, 2015, **4**, 28251-28257. doi: 10.1039/C5RA00023H
  35. Agrawal, M.; Jain, A.; Sridhara Rao, D.V.; Pandey, A.; Goyal, A.; Kumar, A.; Lamba, S.; Mehta, B.R; Muraleedharan, K. & Muralidharan, R. Nano harvesting of GaN nanowires on Si (211) substrates by plasma-assisted molecular beam epitaxy. *J. Crystal Growth* 2014, **402**, 37–41. doi: 10.1016/j.jcrysgro.2014.05.004
  36. Sridhara Rao, D.V. A simple technique for estimation of the voltage of a transmission electron microscope. *J. Electron Microscopy*, 2008, **1**(0), 1–4.
  37. Sridhara Rao, D.V.; Balamuralikrishnan, R. & Muraleedharan, K. Estimation of the voltage of transmission electron microscope (TEM) by <012> CBED-HOLZ analysis using GaAs crystal. *Bull. Mater. Sci.*, 2004, **27**(5), 471. doi: 10.1007/BF02708566
  38. Sridhara Rao, D.V. Transmission electron microscopy studies of GaAs based epitaxial layers. Department of Physics, Indian Institute of Technology, Delhi, December 2005. PhD Thesis,
  39. Stadelmann, P. JEMS (Electron Microscopy Software, Version 1.0724W2001)
  40. Holec, D.; Sridhara Rao, D.V. & Humphreys, C. J. HANSIS software tool for the automated analysis of HOLZ lines. *Ultramicroscopy*, 2009, **109**, 837-844. doi: 10.1016/j.ultramic.2009.03.026
  41. Cockayne, D. Better vision with electron lenses. *Nature Materials*, 2002, **1**, 7-8. doi: 10.1038/nmat717
  42. Missous Mohamed. Fundamental issues of device relevant low-temperature GaAs and related materials properties. *Mat. Sci. Engg. B*, 1997, **44**, 304-310. doi: 10.1016/S0921-5107(96)01762-X
  43. Rosenauer, A.; Kaiser, S.; Reisinger, T.; Zweck, J.; Gebhardt, W. & Gerthsen, D. Digital analysis of high resolution transmission electron microscopy lattice images. *Optik*, 1996, **102**(2), 63-69.
  44. Paul Robb, D. & Alan J., Craven. Column ratio mapping: A processing technique for atomic resolution high-angle annular dark-field (HAADF) images. *Ultramicroscopy*, 2008, **109**, 61–69. doi: 10.1016/j.ultramic.2008.08.001

## ACKNOWLEDGEMENTS

The encouragement of former and present Directors of DMRL, SSPL and former and present CEOs of GAETEC for this research is acknowledged. Also, thanks are due to MBE/MOCVD and device processing groups at SSPL, especially Dr S. Lamba and Dr A. Jain, for providing the specimens for TEM investigations and M/s FEI for HAADF images. The kind support of former group heads of EMG, DMRL is also acknowledged. The authors sincerely thank Prof. A. Rosenauer, University of Bremen, Germany and Prof. A.J. Craven, University of Glasgow, United Kingdom for providing the DALI software and column-ratio mapping softwares respectively. DVSR acknowledges Prof. Sir C.J. Humphreys for interactions on GaN electron microscopy.

## CONTRIBUTORS

**Dr D.V. Sridhara Rao**, Scientist 'F', Defence Metallurgical Research Laboratory, Hyderabad, obtained his MTech (Solidstate Materials) and PhD from IIT, Delhi. He did post-doctoral research in the Department of Materials Science and Metallurgy, University of Cambridge, U.K. He is a life member of IIM, EMSI, MSI and MRSI. He is primarily responsible for the TEM investigations presented in this article.

**Dr R. Sankarasubramanian** obtained his ME in Metallurgy from Indian Institute of Science, Bengaluru. Subsequently he got a PhD, from the same institute before joining Defence Metallurgical Research Laboratory (DMRL), Hyderabad, in 2002. He is currently continuing to be in DMRL and has been primarily focusing on Materials Modeling through Multiscale Multiphysics Simulation Methods. He is responsible for the quantitative HRTEM studies (DALI analysis and column ratio analysis). Also, he has gone through the entire manuscript.

**Mr Deepak Kumar** is a Technical officer in Defence Metallurgical Research Laboratory, Hyderabad. He obtained his BTech in Metallurgical Engineering from Indian Institute of Metals. He has contributed the in-situ SEM experiments and TEM specimen preparation.

**Mr Vajinder Singh**, Scientist 'D', Defence Metallurgical Research Laboratory, Hyderabad, obtained his MTech (Materials Science and Engineering) from Thapar University, Patiala. He has expertise in SEM and EBSD techniques and research interests in the areas of thin films, polymer based composites, high temperature ceramic materials, Ni base superalloys, Titanium alloys and nanomaterials. He is currently pursuing PhD in IIT, Hyderabad. EBSD studies of GaN thin films were his contributions.

**Dr K. Mahadeva Bhat**, Scientist 'F', Solid State Physics Laboratory, obtained his MSc from Mangalore University and PhD from IIT, Chennai. GaAs MMIC technology, GaAs mHEMTs and pHEMTs are his research interests. He has contributed the samples of GaAs pHEMTs and mHEMTs.

**Dr P. Mishra** received her MSc and PhD in Physics from IIT, Delhi. She worked in the University of Electro-Communications, Tokyo, Japan from 1999 to 2003. She is currently a senior scientist at Solid State Physics Laboratory, Delhi. Her current research interests include MBE growth of Antimonide and Arsenide based materials for application in infrared devices. GaSb thin films presented in this paper were grown by her. Also, she has gone through the entire manuscript.

**Dr S. Vinayak**, Scientist 'G', Solid State Physics Laboratory, Delhi, obtained her PhD from IIT, Delhi. Nichrome thin films and Ohmic metallised GaN samples were grown in her research laboratory. Also, she has gone through the entire manuscript.

**Dr T. Srinivasan** is a senior scientist at Solid State Physics Laboratory, Delhi and is doing research and development on III-V quantum hetero-structures for semiconductor devices applications. He has obtained his PhD in physics from IIT Madras, Chennai and was an Assistant Research Engineer at SEAS, UCLA, USA before joining at SSPL. Currently he is looking after III-V MBE division at SSPL. The specimens of low-temperature GaAs and InGaAs quantum dots were grown in his lab.

**Ms R. Tyagi**, Scientist 'G', Solid State Physics Laboratory, Delhi, has research interests in the field of MOCVD growth of III-V compound semiconductor thin films. She has contributed the GaN specimens for EBSD investigations. Also, she has gone through the entire manuscript.

**Dr K. Muraleedharan**, Director, CSIR-Central Glass and Ceramic Research Institute (CGCRI), Kolkata. Earlier, he was the group head, electron microscopy, DMRL and Director of Materials, DRDO HQRS. He obtained PhD in Metallurgy from BHU and pursued post-doctoral research in Carnegie Mellon University, USA. He was instrumental in initiating the joint activity with SSPL on electronic materials. Also, he conceived several electron microscopy experiments, viz., CBED, HRTEM and DF imaging techniques, which are presented in this article.

**Mr R. Muralidharan** was former Director, Solid State Physics Laboratory, Delhi and former Chief Executive Officer, Gallium Arsenide Enabling Technology Centre, Hyderabad. Currently, he is a visiting professor, CeNSE, IISc. His research interests include GaAs, GaN, solar cells, MEMS and MBE growth. He conceived the growth experiments of InGaAs quantum dots, GaAs buffers and GaN HEMTs. Also, he played a key role in the joint activity between DMRL and SSPL on electronic materials, part of which is presented in this article. Also, he has gone through the entire manuscript.

**Mr D. Banerjee** was former Director, DMRL and former Chief Controller (R&D AMS), DRDO. He is currently a Professor in the Department of Materials Engineering, IISc. He has a wide spectrum of research interests, including intermetallics, nickel base superalloys, electronic materials and advanced electron microscopy techniques. He mentored the DMRL-SSPL joint activity on electronic materials. Also, he has gone through the manuscript.